Chang'e-2 spacecraft observations of asteroid 4179 Toutatis

Jianghui Ji[1], Yun Jiang[1], Yuhui Zhao[1], Su Wang[1] and Liangliang Yu[1,2]

[1]Key Laboratory of Planetary Sciences, Purple Mountain Observatory,
Chinese Academy of Sciences, Nanjing 210008, China
[2]Lunar and Planetary Science Laboratory, Macau University of Science and Technology,
Taipa, Macau
email: jijh@pmo.ac.cn

Abstract. On 13 December 2012, Chang'e-2 completed a successful flyby of the near-Earth asteroid 4179 Toutatis at a closest distance of 770 meters from the asteroid's surface. The observations show that Toutatis has an irregular surface and its shape resembles a ginger-root of a smaller lobe (head) and a larger lobe (body). Such bilobate shape is indicative of a contact binary origin for Toutatis. In addition, the high-resolution images better than 3 meters provide a number of new discoveries about this asteroid, such as an 800-meter depression at the end of the large lobe, a sharply perpendicular silhouette near the neck region, boulders, indicating that Toutatis is probably a rubble-pile asteroid. Chang'e-2 observations have significantly revealed new insights into the geological features and the formation and evolution of this asteroid. In final, we brief the future Chinese asteroid mission concept.

Keywords. minor planets, asteroids

1. Introduction

Asteroid 4179 Toutatis was first discovered in 1934 and observed once again in 1989. The asteroid is an Apollo-type Near-Earth Object (NEO) that moves on a near 1:4 resonant orbit with Earth. Thus, ground-based telescopes, especially radar facilities, performed extensive observations when Toutatis approached Earth every four years since 1992. Radar observations acquired from Arecibo and Goldstone during the past two decades show that Toutatis bears an irregular shape with two distinct lobes. Optical and radar measurements further reveal that Toutatis is a non-principal axis (NPA) rotating asteroid, which may result from Earth-approaching flybys in the dynamical evolution (Ostro *et al.* 1995, Hudson & Ostro 1998, Ostro *et al.* 1999, Ostro *et al.* 2002, Hudson *et al.* 2003, Busch *et al.* 2011).

Using higher resolution delay-Doppler radar observations, Hudson & Ostro (1995), Hudson *et al.* (2003) and Busch *et al.* (2012) established Toutatis' 3-dimensional shape models. The dimensions along three principal axes were determined to be 1.92, 2.40 and 4.60 kilometers, respectively. Toutatis was believed to rotate around long-axis with a period of 5.41 days and the long-axis precesses with a period of 7.35 days (Busch *et al.* 2010). Moment of inertia ratios were evaluated to be 3.22 ± 0.01 and 3.09 ± 0.01 (Ostro *et al.* 1999). Recently, Takahashi *et al.* (2013) modeled the rotational dynamics and evaluated the spin state parameters of Toutatis with radar data spanning from 1992 to 2008, and they showed that the solar and terrestrial gravitational tidal torques can play a role in affecting its angular momentum.

As an NEO originates from the main belt, Toutatis, which was a suitable target for the Chang'e-2 flyby mission, may provide key clues on the formation of the Solar system. In addition, Toutatis appears to be the largest Potential Hazardous Asteroids (PHAs) which
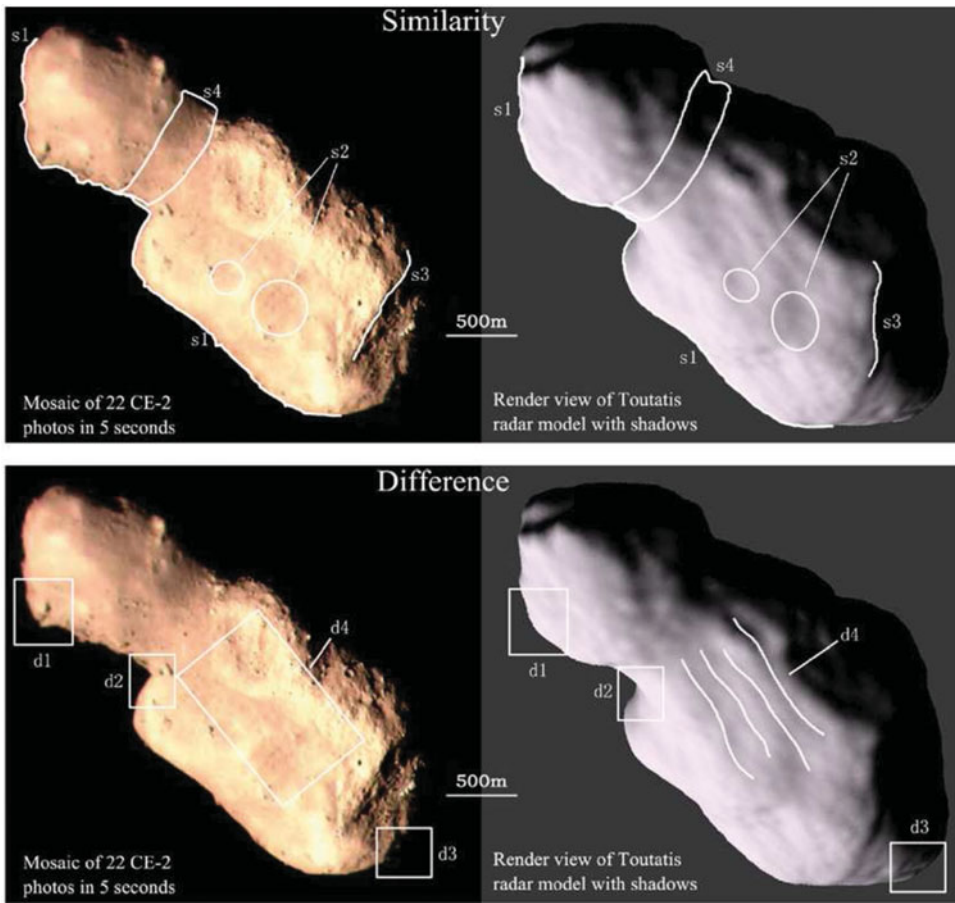
Figure 1. Comparison of Toutatis' geological features between optical images acquired by Chang'e-2 (color, left) and the radar model (gray, right) by Hudson *et al.* (2003). Similarities (s1-s4) and differences (d1-d4) are marked. This figure is reproduced from Zou *et al.* (2014).

is full of enigmas - it is a NPA rotator with a bilobate shape (Ostro *et al.* 1995, Hudson *et al.* 2003) and may have a rubble pile structure. The flyby mission confirmed the radar model's double-lobed appearance of Toutatis, and optical images acquired provide new insights on the origin and evolution of the asteroid (Huang *et al.* 2013a).

Chang'e-2, as the second Chinese spacecraft to the Moon's exploration, was launched on 1 October 2010. During the mission, the probe orbited the Moon for six months. High-resolution images of the lunar surface were obtained for studying Moon's morphology. After the successful mission around the Moon, Chang'e-2 departed its orbit on 9 June 2011 and moved its way to the Sun-Earth Lagrangian point (L2) for exploring the space environment. It arrived L2 on 25 August 2011. Subsequently, on 12 December 2012, the asteroid would move to the closest approach to the Earth. After over 230 days stay at L2, Chang'e-2 started its mission to Toutatis† on 1 June 2012 and on 13 December 2012

† Before the flyby mission, the ground-based observation campaign for Toutatis was sponsored by the Chinese Academy of Sciences from May to November in 2012. We collected the observations from the Minor Planet Center as well as those from the observation campaign to refine the orbit of Toutatis, with uncertainties on the order of a few kilometers (Huang *et al.* 2013a, Huang *et al.* 2013b).
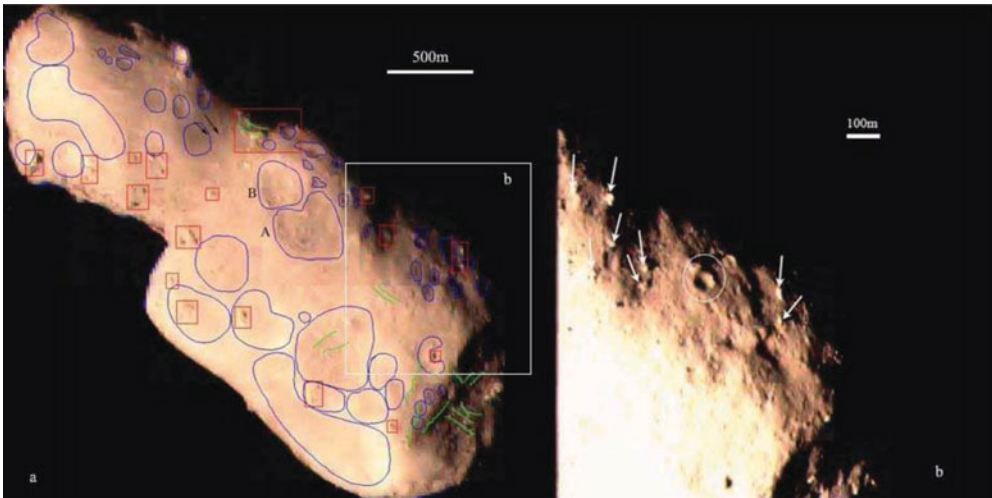
Figure 2. Various geological features on the surface of Toutatis. (a) Craters (blue circles), boulders (red squares), lineaments (green lines) as well as the flow direction of regolith (black arrows) are outlined. (b) A morphological-integrity crater shows a sharp bowl shape, with dozens of boulders distributing around. This figure is reproduced from Huang *et al.* (2013a).

the spacecraft had a closest miss at about 770 ± 120 (3σ) meters from Toutatis' surface (Huang *et al.* 2013a). It was the first time that the images of Toutatis were acquired so closely. There were about 425 images obtained. The highest resolution images of Toutatis are better than 3 m pixel^{-1}. Now Chang'e-2 is still alive and flying to the space far away from Earth, more than 100 million kilometers in a heliocentric orbit.

In this work, we review the results of Toutatis as observed from the Chang'e-2 flyby mission. Section 2 describes the surface geological features of Toutatis. The orientation and rotational parameters of Toutatis are determined in combination of the optical images of Chang'e-2 and radar measurements in Section 3. The formation scenarios are discussed in Section 4. In final, future Chinese asteroid mission is introduced in Section 5.

2. Surface Geological Features

The Chang'e-2 flyby allows for observing the morphology of $\sim 45\%$ surface of Toutatis. Figure 1 shows that both the optical images acquired by Chang'e-2 and the radar-derived shape model exhibit similar silhouette (s1), two circular concavities in the middle area of body (s2), a scarp (possibly crater rim) with similar length and slope (s3) and the joint part with similar width, shape and location (s4)(Zou *et al.* 2014). However, several differences also exist: d1. A small angular feature appears visible on the profile of head in the flyby image, which is vaguely shown in the radar model. d2. A perpendicular profile near the neck region is sharp in the image but vague in the model. d3. The far side of the big lobe is longer in the model, and is flatter in the image. d4. Four striations lie on the middle area in the direction parallel to the Z-axis (long axis) in the shape model but not in the image (Zou *et al.* 2014). Moreover, Toutatis' dimensions estimated from the radar model ($x = 4.60 \pm 0.10 \ km, z = 1.92 \pm 0.10 \ km$) is a bit smaller than those $[(4.75 \times 1.95 \ km) \pm 10\%]$ given by the spacecraft images (Hudson *et al.* 2003; Huang *et al.* 2013a). These similarities and differences can provide significant improvements to the current shape model of Toutatis (Busch *et al.* 2014).

From flyby images, Toutatis is observed to be covered by abundant concavities, indicating that impact cratering may play an important role in shaping the present surface.
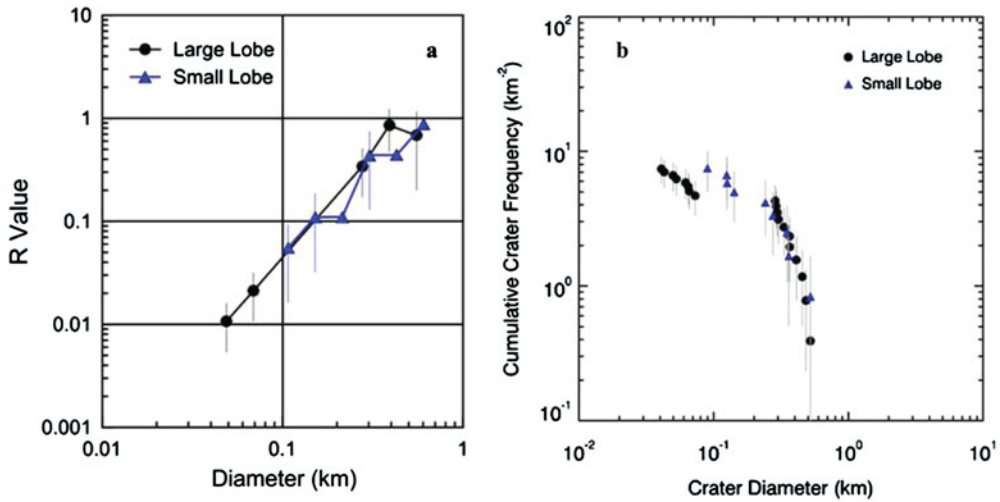
Figure 3. The relative (a) and cumulative (b) size-frequency distribution for craters on Toutatis (Huang *et al.* 2013a).

Fresh impact craters have been defined as "circular rimmed depressions" (Melosh 2011). However, the overall quality of optical images is relatively poor because they were captured by the monitoring camera. In addition, the high solar phase angle is not conducive to accurate topographic analyses. All these factors make the identification of craters on the imaged side of Toutatis difficult and incompatible for different researchers. Thus, different numbers of craters have been counted (Huang *et al.* 2013a; Zou *et al.* 2014; Zhu *et al.* 2014). According to Huang *et al.* (2013a), approximately fifty craters have been identified from 36 to 532 m in size. Most large craters show shallow depths and obscure shapes, which may result from resetting process (Chapman *et al.* 2002). For instance, seismic shaking from subsequent impacts can cause regolith displacement to erase craters' rims. In addition, Zhu *et al.* (2014) regarded the giant depression ($\sim$ 800 m) at the big end as a crater. However, Huang *et al.* (2013a) suggested that this large-end depression, with relatively subdued relief, is more likely related to the internal structure of body. All craters identified from the given images are labeled in blue profiles in Figure 2. Figure 3 shows that the cumulative size-frequency distributions indicate that two lobes may undergo either similar history in the cratering (Huang *et al.* 2013a), or the big lobe may suffer from more impacts than the small one (Zou *et al.* 2014). Assuming a solid impactor and proper scaling law, Zhu *et al.* (2014) estimated the energy of the impactor for the 800 m depression at the big end to be 5×10^{11} J. This result is fairly greater than the energy required for breaking up a bulk rock with the same size of Toutatis. Therefore, they inferred that Toutatis might not bear a monolithic structure but a rubble pile with fragments accreted. In addition, they calculated the seismic attenuation factor $\alpha = 1.43$ for the largest depression at the big end of Toutatis, which is higher than those of other porous asteroids. This may greatly attenuate the heavy shock wave so that abundant large craters are unlikely to lead to global disruption of Toutatis (Zhu *et al.* 2014).

Boulders show a clearly identifiable brightness variation as well as a bright positive relief with shadow next to it, according to the criteria of boulders on the surface of Lutetia (Küppers *et al.* 2012). More than 200 boulders scattered across its surface have been counted over the imaged area of Toutatis (Figure 2). Note that the boulder size with geometric mean in this work is smaller than the value with maximum size measured in the previous study (Huang *et al.* 2013a; Zou *et al.* 2014), mainly due to the deviations in
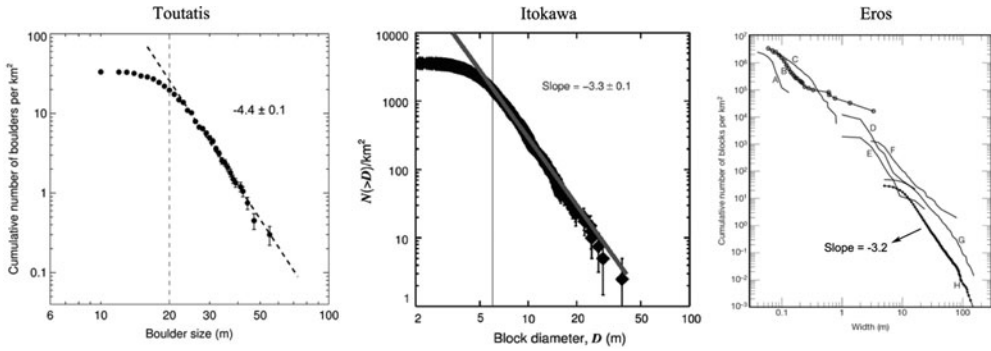
Figure 4. A comparative view of cumulative size-frequency distribution (SFD) of boulders of Toutatis, Itokawa and Eros, which are reproduced from Jiang *et al.* (2015a), Mazrouei *et al.* (2014) and Thomas *et al.* (2001), respectively.

the measurement of boulder size. As a result, boulders have dimensions ranging from 10 to 61 m, with an average size of 22 m and 90% of them less than 30 m. The two largest boulders (> 50 m) are about the neck region. The cumulative boulder size frequency distribution exhibits a slope of -4.4 $\pm$ 0.1 for 20-60 m size, which is much steeper than slopes of -3.3 $\pm$ 0.1 for Itokawa boulders with 6-38 m size and of -3.2 for Eros boulders with 15-80 m size (Thomas *et al.* 2001; Mazrouei *et al.* 2014) (Figure 4). Moreover, like Itokawa, Toutatis is most likely of rubble-pile origin, where most boulders are probably fragments from the parent body but are not generated by impact cratering as for Eros (Jiang *et al.* 2015a; see also Jiang *et al.* 2015b, this volume). Troughs and ridges are the major types of linear structures observed from the flyby images. The origin of the troughs on the surface may arise from the impact of other asteroids.

The optical images of Toutatis acquired by Chang'e-2 spacecraft show that a handful of small craters have fresh and sharp bowl-shapes, with upheaval rims without rays, indicative of impacts on loose regolith. Those large craters with subdued rims and smooth floors also indicate the existence of fine-grained regolith on the surface of Toutatis (Huang *et al.* 2013a; Zhu *et al.* 2014). Ostro *et al.* (1999) surmised that regolith with porosity of lunar soils should exist and cover nearly one third of the surface of Toutatis based on their radar observations. As known, the estimation of the thermal inertia of asteroids' surface can provide a more effective and reliable way to discern the presence of regolith, as a low surface thermal inertia generally suggests a regolith surface. Howell *et al.* (1994) estimated the thermal inertia of Toutatis to be $300 \sim 800$ Jm^{-2}K^{-1}s$^{-0.5}$ by employing the thermophysical model to reproduce a 3 μm spectral region of Toutatis. In addition, using the statistical relationship between asteroid's thermal inertia and effective diameter (Delbo' *et al.* 2007), the surface thermal inertia of Toutatis can be estimated to be $150 \sim 225$ Jm^{-2}K^{-1}s$^{-0.5}$, which seems to be quite similar to that of Eros ~ 150 Jm^{-2}K^{-1}s$^{-0.5}$, but much lower than that of Itokawa ~ 750 Jm^{-2}K^{-1}s$^{-0.5}$. Although the above estimation may be rough, it can still work as a reference to infer the surface situation of the asteroid. As described above, Toutatis may have a much lower thermal inertia than that of Itokawa, implying that the coverage of regolith layer over Toutatis' surface is much more widely than that on Itokawa's surface.

3. Dynamics and Orientation

Using the radar data obtained during 1992 flyby, Ostro *et al.* (1995) presented a spin period between 4 and 5 days. Hudson & Ostro (1995) used a least-squares estimation to

calculate the two major periods, which were found to be 5.41 days for rotation about the long axis and 7.35 days for precession of the long axis about the axis of angular momentum vector. Subsequently, Toutatis was observed by Goldstone during its 1996 approach. Ostro *et al.* (1999) further showed that the two periods of Toutatis to be 5.376 ± 0.001 and 7.420 ± 0.005 days, respectively, by analyzing the radar measurements. Scheeres *et al.* (2000) suggested that the tumbling spin state of Toutatis might be a result of near-Earth flybys over its lifetime. Recently, Takahashi *et al.* (2013) modeled the rotational dynamics and calculated Toutatis' rotational parameters using radar observations of five flybys from 1992 to 2008.

Based on the optical results by Chang'e-2, Zou *et al.* (2014) calculated the imaging distances and image resolutions, and used profile contour and the similarity method to measure the attitude angles related to the view port of the imaging camera, further showed that the contour matching results are $\alpha = $ -33.8°, $\beta = 33.0°$, $\gamma = 47.1°$, in the form of 3-1-2 Euler angles. According to the graphical frame described with the angles of direction $\cos i$ near the flyby epoch, Bu *et al.* (2015) rotated the radar model and derived the orientation of $126.13° \pm 0.29°$, $122.98° \pm 0.21°$ and $126.63° \pm 0.46°$, without considering the attitude of the camera in the inertia frame.

Zhao *et al.* (2015a) employed four frameworks to determine the orientation of Toutatis at the flyby epoch. Radar-derived models are rotated about three principal axes to match the optical images. In combination of the spacecraft's attitude and camera information, the matching results are adopted to evaluate Toutatis' rotational parameters through a shooting process. The three of 3-1-3 form Euler angles from body-fixed frame to inertial coordinate system are $\alpha = -32° \pm 5°$, $\beta = -50° \pm 0.8°$, and $\gamma = 12° \pm 5°$, respectively.

Figure 5 shows that the variations in the angular momentum originate from all external gravitational torques, and that of Earth, Moon, and Jupiter and Saturn, respectively (Zhao *et al.* 2015a, see also Zhao *et al.* 2015b, this volume). The first order of external gravitation torque is proven to be ignorable (Zhao *et al.* 2015a). Solar tides play a prominent role in all external perturbations acting on Toutatis' rotational status for the past two decades. An apparently 1:4 resonance is figured out from the torque variation curves caused by the Earth and Moon. Regular variations in Jupiter's tidal effects is generated by the 3:1 mean motion resonance with Jupiter. Figure 5 shows the angular momentum variations that Toutatis experienced due to the Earth and Moon gravity during the 2004 close approach to Earth. The angular momentum orientation of Toutatis is determined to be $\lambda_H = 180.2^{+0.2°}_{-0.3°}$ and $\beta_H = -54.75^{+0.15°}_{-0.10°}$. Toutatis is evaluated to spin along long-axis with a period of 5.38 days and the long-axis precesses with a period of 7.40 days (Zhao *et al.* 2015a), which is in consistence with the previous outcomes (Hudson & Ostro 1995, Hudson *et al.* 2003).

4. Formation Scenario

The Chang'e-2 flyby to Toutatis provides us new observations to understand the formation scenario of asteroids. As the previous investigations shown, Toutatis is an S-type asteroid that probably has a rubble-pile structure. Using the density of L ordinary chondrites, ~ 3.34 g cm^{-3} (Scheeres *et al.* 1998), and typical density of S-type asteroids, 2.1-2.5 g cm^{-3} (Reddy *et al.* 2012), Toutatis' porosity is suggestive of a value ranging from 25% to 37%. This infers that its porosity is between that of Eros and Itokawa, indicating that Toutatis may be not a monolith but a coalescence of shattered rocks. Furthermore, such structures and the bifurcated configuration of Toutatis also imply that this asteroid is catalogued as a contact binary, which refers to a sort of asteroid containing two lobes in contact (Benner *et al.* 2006). Several likely origin mechanisms of contact binaries have
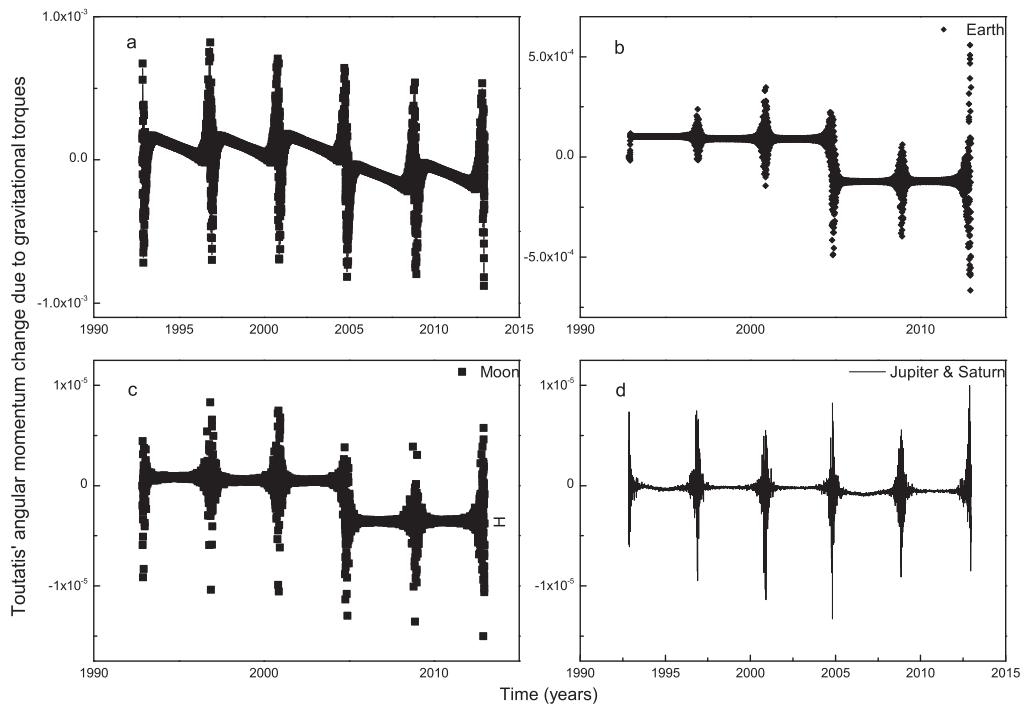
Figure 5. Variations in the angular momentum of Toutatis: (a) all external gravitational torques, that of (b) the Earth, (c) the Moon, (d) Jupiter and Saturn.

been studied (Ćuk 2007, Scheeres 2007, Taylor & Margot 2011), and suggested that two lobes of contact binary may have been separated once and have bimodal mass distribution (Benner *et al.* 2006, Brozovic *et al.* 2010). The bilobate shape of Toutatis is similar to that of Itokawa and the nucleus of the 67P/Churyumov-Gerasimenko (Fujiwara *et al.* 2006, Sierks *et al.* 2015). However, the formation of Toutatis is not fully understood yet.

Recently, several formation scenarios are proposed to produce this bilobate shape like Itokawa: (1) two detached objects colliding with a relatively low speed; (2) two components from the identical parent body undergoing re-impact and recombination due to YORP and Binary YORP (Mazrouei *et al.* 2014);(3) tidal disruption from a terrestrial planet (Fujiwara *et al.* 2006) and catastrophic collisions (Huang *et al.* 2013a and references therein), etc. As above-mentioned, the nucleus of 67P/Churyumov-Gerasimenko also consists two lobes, the body, head and the neck conjunction. There are mainly two scenarios for the formation of such kind of comet: hierarchical accretion and accumulation of planetesimals. When it formed, 67P/Churyumov-Gerasimenko is a contact binary which bears a resemblance to Toutatis (Sierks *et al.*, 2015). Hence, Toutatis, as well as Itokawa and 67P/Churyumov-Gerasimenko, seems to suffer from similar formation process.

5. Future Mission

Chang'e-2 observations have significantly shed new insights into the morphological features (such as the large depression in the big end, the sharply perpendicular profile, the distribution of the craters and boulders) for Toutatis. These observations can help us understand the formation scenarios of this kind of asteroid, which could provide clues

to unveiling the formation of population of contact binary. Moreover, future Chinese asteroid mission (Multiple Asteroids Rendezvous and in-situ Survey (MARS) Mission) will sequently visit three NEOs: (99942)Apophis (Binzel *et al.* 2009, Souchay *et al.* 2014), and (175706)1996 FG3 (Pravec *et al.* 1998, Pravec *et al.* 2000, Mottola & Lahulla 2000, Yu *et al.* 2014, Scheirch *et al.* 2015) are potential candidates. There are seven scientific payloads proposed on board, e.g., multi-spectral imager, panoramic camera, penetrating radar, near infrared spectrometer, gamma-ray spectrometer, in-situ sampling and analyzer, and ion energy spectrum imager. MARS mission will be hopeful to provide the key to the formation of planets, the evolution of Solar system and the origin of life on the Earth.

Acknowledgements

References

Abe, M. *et al. Science*, 312:1334–1338, 2006
Benner, L. A. M. *et al. Icarus*, 182:474–481, 2006
Binzel, R. P. *et al. Icarus*, 200:480–485, 2009.
Brozovic, M. *et al. Icarus*, 208:207–220, 2010.
Bu Y. L., *et al. AJ*, 149:21, 2015.
Busch, M. W. *et al. Icarus*, 209:535–541, 2010.
Busch, M. W. *et al. EPSC-DPS2011*, 6:297, 2011.
Busch, M. W. *et al. 2012 AGU Fall Meeting*, P31A-1873, 2012.
Busch, M. W. *et al. 2014 Asteroids, Comets, Meteors Meeting*, 69, 2014.
Chapman, C. R. *et al. Icarus*, 155:104–118, 2002.
Ćuk, M. *ApJL*, 659:57–60, 2007.
Delbo', M., *et al. Icarus*, 190:236–249, 2007
Dunn, T. L. & Burbine, T. H. *Lunar Planet. Sci.*, 43, March 19–23, 2012, The Woodlands, Texas. LPI Contribution No. 1659, ID 2305
Fujiwara, A., Kawaguchi, J., Yeomans, D. *et al. Science*, 312:1330–1334, 2006
Howell, E. S., Britt, D. T., Bell, J. F., *et al. Icarus*, 111:468–474, 1994
Huang, J. C. *et al. Scientfic Reports*, 3:3411–3416, 2013a.
Huang, J. C. *et al. Science China Technological Sciences*, 43:596–601, 2013b.
Hudson, R. S. & Ostro, S. J. *Science*, 270:84–86, 1995.
Hudson, R. S. & Ostro, S. J. *Icarus*, 135: 451–457, 1998.
Hudson, R. S., Ostro, S. J., & Scheeres, D. J. *Icarus*, 161:346–355, 2003.
Jiang, Y., *et al.* accepted to *Scientific Reports*, 5: 16029, 2015a.
Jiang, Y., *et al.* accepted to *Proceedings IAU Symposium No. 318*, 153–155, 2015b.
Küppers, M. *et al. Planet. Space. Sci.*, 66:71–78, 2012.
Mazrouei, S., *et al. Icarus*, 229:181–189, 2014.
Melosh, H. J. Planetary Surface Processes. Cambridge University Press, Cambridge, 2011.
Michikami, T. *et al. Earth Planets Space*, 60:13–20, 2008.
Mottola, S., & Lahulla, F. *Icarus*, 146:556–567, 2000.
Ostro, S. J. *et al. Science*, 270:80–83, 1995.
Ostro, S. J., *et al. Icarus*, 137:122–139, 1999.

Ostro S. J., *et al.*, 2002, Asteroids III, Univ. of Arizona Press, Tucson: 151

Pravec, P., Wolf, M., & Lenka, S. *Icarus*, 133:79–88, 1998.

Pravec, P. *et al. Icarus*, 146:190–203, 2000.

Reddy, V. *et al. Icarus*, 221, 1177-1179, 2012

Scheeres, D. J. *et al. Icarus*, 132:53–79, 1998.

Scheeres, D. J. *et al. Icarus*, 147:106–118, 2000.

Scheeres, D. J. *Icarus*, 189:370–385, 2007.

Scheirch, P. *et al. Icarus*, 245:56–63, 2015.

Sierks, H., Barbieri, C., Lamy, P. L. *et al. Science*, 347:aaa1044, 2015.

Souchay, J. *et al. A&A*, 563:24, 2014.

Takahashi, Y., Busch, M. W. & Scheeres, D. J. *AJ*, 146:95, 2013.

Taylor, P. A. & Margot, J-L *Icarus*, 2112:661-676, 2011.

Thomas, P. C., Veverka, J., Robinson, M. S. & Murchie, S. *Nature*, 413:394-396, 2001.

Yu, L. L., Ji, J. H., & Wang, S. *MNRAS*, 439:3357–3370, 2014.

Zhao, Y. H. *et al. MNRAS*, 450:3620, 2015a.

Zhao, Y. H. *et al. submitted to Proceedings IAU Symposium No. 318*, 156–159, 2015b.

Zhu, M. H. *et al. Geophys. Res. Lett.*, 41:328–333, 2014.

Zou, X. D. *et al. Icarus*, 229:348–354, 2014.